ACS OMEGA

Article

Cite This: ACS Omega 2019, 4, 5117−5125

http://pubs.acs.org/journal/acsodf

Fe_3O_4 Nanoparticles Grown on Cellulose/GO Hydrogels as Advanced Catalytic Materials for the Heterogeneous Fenton-like Reaction

Yian Chen,[†,§] Petra Pötschke,*[,†] Jürgen Pionteck,[†] Brigitte Voit,[†,§] and Haisong Qi*[,‡]

[†]Leibniz-Institut für Polymerforschung Dresden e. V. (IPF), Hohe Straße 6, D-01069 Dresden, Germany

[‡]State Key Laboratory of Pulp and Paper Engineering, South China University of Technology, 510630 Guangzhou, China

[§]Organic Chemistry of Polymers, Technische Universität Dresden, D-01062 Dresden, Germany

Supporting Information

ABSTRACT: Cellulose/graphene oxide (GO)/iron oxide (Fe_3O_4) composites were prepared by coprecipitating iron salts onto cellulose/GO hydrogels in a basic solution. X-ray photoelectron spectroscopy (XPS), Fourier-transform infrared, and X-ray diffraction characterization showed that Fe_3O_4 was successfully coated on GO sheets and cellulose. Cellulose/GO/Fe_3O_4 composites showed excellent catalytic activity by maintaining almost 98% of the removal of acid orange 7 (AO7) and showed stability over 20 consecutive cycles. This performance is attributable to the synergistic effect of Fe_3O_4 and GO during the heterogeneous Fenton-like reaction. Especially, the cellulose/GO/Fe_3O_4 composites preserve their activity by keeping the ratio of Fe^{3+}/Fe^{2+} at 2 even after 20 catalysis cycles, which is supported by XPS analysis.

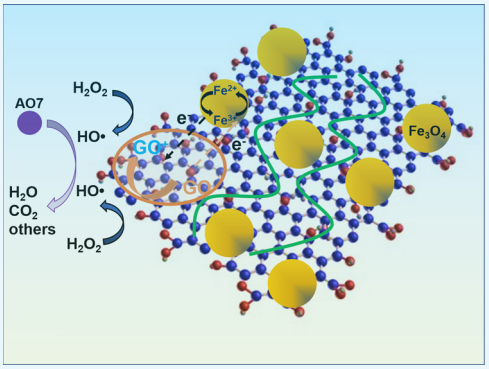

INTRODUCTION

Dye-contaminated wastewaters from textile, plastic, and paper industries cause worldwide attention in the water environment. The textile industry presents a global pollution problem on account of the accidental or dumping discharge of dye waste−water into waterways.[1] To meet stringent environmental regulations, the treatment of dye wastewater is compulsory, enforced, and highly regulated. Advanced oxidation processes (AOPs) are used as an efficient and robust method for the treatment of dye wastewater because of their low toxicity and high degradation performance. AOPs are based on the generation of highly reactive HO$^\bullet$ to degrade organic pollutants.[2] The HO$^\bullet$ radicals are produced by either hydrogen peroxide (H_2O_2) and/or ozone (O_3) whereby ultrasound, light, and temperature can be used to support the process. Oxidation with Fenton- or Fenton-like reactions is a promising process within AOPs, resulting mainly from the generation of HO$^\bullet$ radicals that efficiently and nonselectively degrade organic pollutants.[3,4] However, there are still many disadvantages when applying such homogeneous Fenton- or Fenton-like reactions, such as the restricted experimental conditions, the accumulation of iron hydroxide sludge, and the non-regeneration of the catalyst.[5−7]

In order to overcome these disadvantages of the homogeneous reaction, heterogeneous Fenton-like catalysts were developed as a suitable alternative, which at the same time allows the catalyst to be reused in further cycles. The iron species are commonly immobilized in catalyst supports, such as clay,[8−12] alumina,[13,14] zeolite,[15,16] silica,[17] and carbonaceous materials.[18−21] Therefore, the Fenton or Fenton-like reactions generally occur at the solid−liquid interfaces, where the iron remains substantially in the solid phase either as a mineral or as an adsorbed ion.[18,22] In particular, carbonaceous materials, such as activated carbon (AC),[20,23,24] carbon nanotubes (CNTs),[18,21,25] mesoporous carbon,[26] and carbon aerogels,[20,27] have been well proven as catalyst carriers to immobilize the iron species because of their special performance as a cocatalyst. Recently, Voitko et al.[28] reported that graphene oxide (GO) showed better degradation performance than CNTs and AC, which was attributed to the many oxygen-containing functional groups of the GO plates. Although GO shows great attractiveness to act as a catalyst support, there are very few works reported using GO in heterogeneous Fenton-like catalysts for the degradation of persistent organic pollutants. The main reason is the difficulty in recycling of iron species and the catalyst support. Therefore, embedding iron species onto proper supports to improve their recyclability and stability is an important issue. A step in this direction was taken by Zubir et al.,[29−31] who reported in recent years on the use of GO/Fe_3O_4 nanocomposites to degrade acid orange 7 (AO7). Although the interaction of GO and Fe_3O_4 leads to the stability and great performance in the degradation of AO7, the use of GO as the catalytic support still limits its convenient application as it is difficult to remove the catalyst after the catalytic reaction.

Received: January 18, 2019
Accepted: February 20, 2019
Published: March 11, 2019

DOI: 10.1021/acsomega.9b00170
ACS Omega 2019, 4, 5117−5125

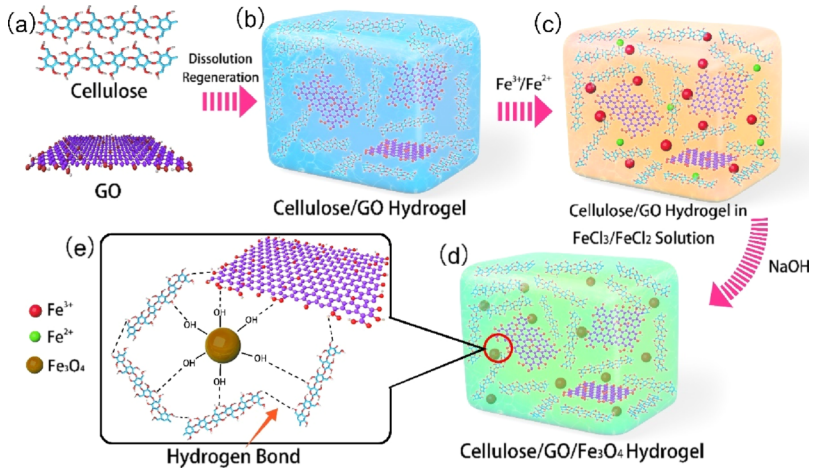

Figure 1. Illustration of cellulose/GO/Fe_3O_4 hydrogel synthesis: (a) cellulose and GO; (b) cellulose/GO hydrogel; (c) cellulose/GO hydrogel in $FeCl_3$/$FeCl_2$ solution; (d) cellulose/GO/Fe_3O_4 hydrogel; (e) multiple hydrogen bonds.

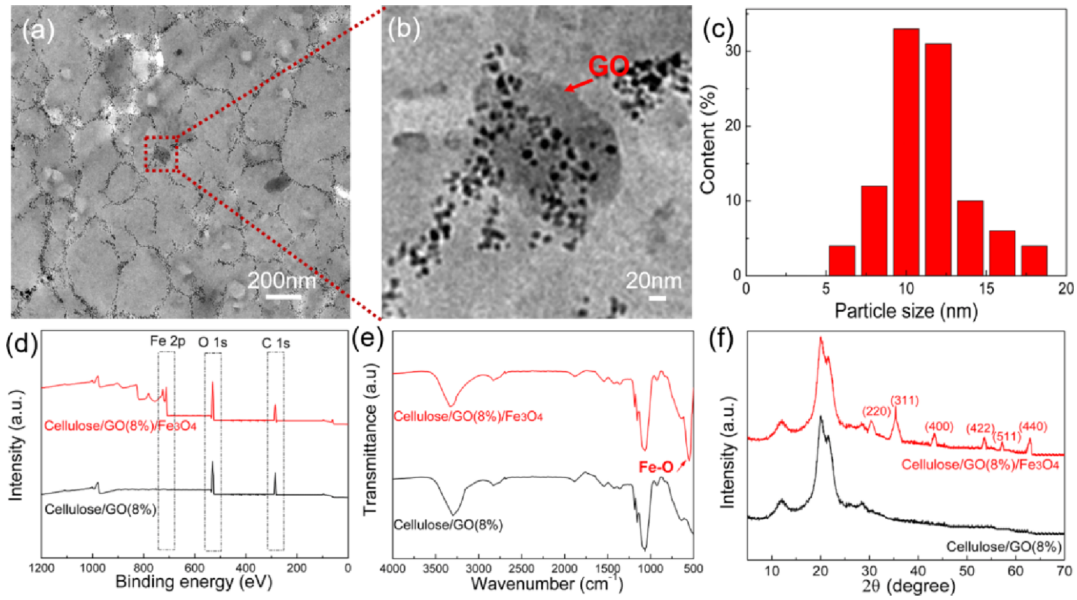

Figure 2. (a) Low magnification and (b) high magnification TEM images of Fe_3O_4 nanoparticles grown on GO sheets. (c) Fe_3O_4 nanoparticles size distribution as determined from TEM micrographs. (d) Wide scan XPS spectra of cellulose/GO (8%) and cellulose/GO (8%)/Fe_3O_4. (e) FTIR spectra of cellulose/GO (8%) and cellulose/GO (8%)/Fe_3O_4. (f) XRD spectra of cellulose/GO (8%) and cellulose/GO (8%)/Fe_3O_4.

This work proposes a novel approach to use cellulose/GO hydrogels as a catalyst support for catalysis, especially in the Fenton-like reaction system. The iron species can be processed into catalytic composite materials based on film or paper, the so-called "dip catalyst". A "dip-catalyst" is characterized by its high recyclability and its convenient use, in particular by the fact that it can switch the reaction on and off almost immediately by immersion/removal in the reaction medium. Such catalytic film-based composites can be prepared by dip-coating cellulose/GO hydrogels with iron ions. As proved in our previous work, we have successfully produced cellulose/GO hydrogel with GO sheets uniformly dispersed within the cellulose matrix. The open network structure formed by cellulose provides ideal conditions for the easy diffusion of Fe^{2+} and Fe^{3+} into the cellulose/GO hydrogel. Thus, Fe_3O_4 can immobilize uniformly onto the GO surface and the cellulose chains, while maintaining the structure of the cellulose matrix. Although, the cellulose matrix contains GO and Fe_3O_4 nanoparticles, it retains the hydrogel structure during the catalyst reaction so that no secondary contamination occurs.

About half of the worldwide production of dyes can be classified as azo compounds that have one or more azo groups (−N═N−) in their molecular structure.[4,6] Among the azo dyes, AO7 is the most widely used dye in the textile manufacturing industry because of its high stability and low cost.[5] Therefore, this dye was used as a model pollutant to study the catalytic performance of cellulose/GO/Fe_3O_4 composites with respect to oxidation in the heterogeneous Fenton-like reaction.

RESULTS AND DISCUSSION

Preparation and Properties of Cellulose/GO/Fe_3O_4 Composites. The preparation of cellulose/GO/Fe_3O_4 composites is shown in Figure 1. We used the NaOH/urea aqueous solution in the first step to prepare the cellulose/GO hydrogel because the NaOH/urea aqueous solution was found

DOI: 10.1021/acsomega.9b00170
ACS Omega 2019, 4, 5117−5125

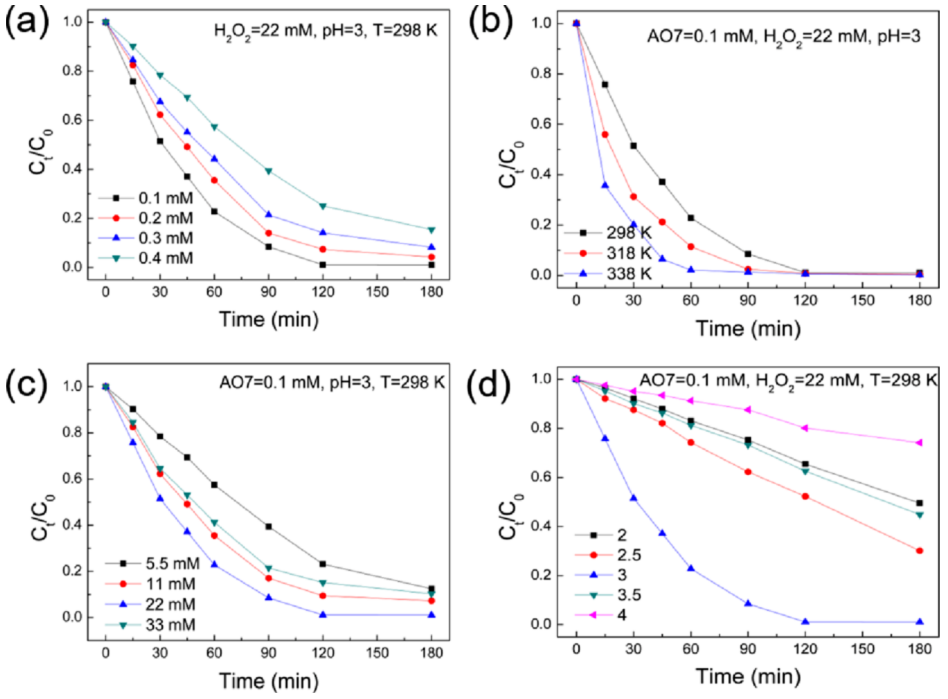

Figure 3. (a) Effect of the initial AO7 concentration on the degradation of AO7 by H_2O_2 catalyzed with the cellulose/GO (8%)/Fe_3O_4 composite. (b) Effect of temperature on the degradation of AO7 by H_2O_2 catalyzed with the cellulose/GO (8%)/Fe_3O_4 composite. (c) Effect of H_2O_2 content for AO7 oxidation by H_2O_2 catalyzed with the cellulose/GO (8%)/Fe_3O_4 composite. (d) Effect of pH on the degradation of AO7 by H_2O_2 catalyzed with the cellulose/GO (8%)/Fe_3O_4 composite.

to facilitate good dispersion of GO in the cellulose matrix, which was sketched in Figure 1b. The proposed generation mechanism of Fe_3O_4 nanoparticles in cellulose/GO hydrogel is shown in Figure 1c,d. When the cellulose/GO hydrogel was immersed in the $FeCl_3/FeCl_2$ solution, Fe^{3+}/Fe^{2+} were adsorbed around the carboxyl and hydroxyl groups of the cellulose and the GO sheets. Afterward, when NaOH was added into the solution, Fe^{3+}/Fe^{2+} were hydrolyzed to generate $Fe(OH)_3/Fe(OH)_2$. After the condensation of $Fe(OH)_3/Fe(OH)_2$, Fe_3O_4 was immobilized in the cellulose/GO hydrogel. Multiple hydrogen bonds formed in the cellulose/GO/Fe_3O_4 hydrogel, as shown in Figure 1e, stabilize the Fe_3O_4 nanoparticle dispersion in the hydrogel.

The results of structural and morphological analysis of cellulose/GO/Fe_3O_4 composites are shown in Figure 2. The cellulose/GO hydrogel as the catalyst support provides ideal conditions for easy diffusion of Fe^{2+} and Fe^{3+} into the hydrogel and their efficient reaction with GO and cellulose. The Fe_3O_4 nanoparticles formed in NaOH were evenly generated on the surface of GO sheets and cellulose chains (Figure 2a,b). The average size of the Fe_3O_4 is 10−13 nm, as depicted in Figure 2c. It is noteworthy that due to the strong chemical interaction between the carboxylate ions and iron oxide,[32] Fe_3O_4 nanoparticles were applied directly to the GO surface and cellulose without molecular links, as shown in Figure 1e.

The prepared composites were further analyzed using wide scan X-ray spectra to confirm the formation of Fe_3O_4 nanoparticles in the cellulose/GO hydrogel. The spectra of cellulose/GO (8%)/Fe_3O_4 shows photoelectron lines at binding energies of 285, 530, and 711 eV, which are attributed to C 1s, O 1s, and Fe 2p, respectively. More detailed XPS information of different composites is shown in Figure S1a. In the high resolution Fe 2p scan (Figure S1b), the binding energy peaks at 724.7 and 711.2 eV correspond to Fe $2p_{1/2}$ and Fe $2p_{3/2}$, respectively. The generation of Fe_3O_4 nanoparticles can be confirmed by the disappearance of the charge-transfer satellite of Fe $2p_{3/2}$ at about 720 eV.[33,34] The formation of Fe_3O_4 nanoparticles was also confirmed by Fourier-transform infrared (FTIR) spectroscopy (Figure 2e). For cellulose/GO (8%)/Fe_3O_4 composite, there is an extra band at around 584 cm^{-1}, which is attributed to Fe−O. The crystal structure of Fe_3O_4 nanoparticles was confirmed by the presence of diffraction peaks at 2θ = 30.3° (220), 35.4° (311), 43.3° (400), 53.6° (422), 57.2° (511), and 62.9° (440) in Figure 2f. All the peaks in the X-ray diffraction (XRD) patterns of Fe_3O_4 nanoparticles are consistent with reports in the literature.[35,36] Figure S2a shows the thermal stability of the composite films. The Fe_3O_4 nanoparticle content can be calculated by the residue of composite films with and without Fe_3O_4 (Figure S2b). The Fe_3O_4 nanoparticle content of the different cellulose/GO/Fe_3O_4 composite was not affected by the content of GO in the cellulose/GO/Fe_3O_4 composites and is around 12 wt %.

Optimization Analysis of the AO7 Degradation Conditions. The catalytic performance of cellulose/GO/Fe_3O_4 composites was assessed on the basis of their reactivity to the oxidation of AO7 as a model pollutant in the heterogeneous Fenton-like reaction. In this part, using cellulose/GO (8%)/Fe_3O_4 hydrogel as the catalyst, the optimization of the experimental conditions for the AO7 oxidation was performed, including the effects of the initial AO7 dye concentration, temperature, pH, and the initial concentration of H_2O_2. Figure 3a shows the relationship between the initial AO7 dye concentration and the degradation of AO7. As the AO7 dye content increased, the degradation activity obviously slowed down. The high AO7 concentration leads to inductive effects and the active sites of the cellulose/GO (8%)/Fe_3O_4 hydrogel were covered by excess AO7. Thus,

DOI: 10.1021/acsomega.9b00170
ACS Omega 2019, 4, 5117−5125

it can limit the generation of $HO^{\bullet}$ from H_2O_2 at the active sites of the cellulose/GO (8%)/Fe_3O_4 hydrogel.

Figure 3b illustrates the influence of temperature on the AO7 oxidation. Fast rates could be observed and 64% degradation was reached within 15 min at 338 K. In contrast, it takes 45 min at 298 K. Obviously, high temperature increases the mobility of H_2O_2 and AO7 to the surface of the cellulose/GO (8%)/Fe_3O_4 hydrogel, thereby resulting in more $HO^{\bullet}$, thus accelerating the degradation of AO7. Nevertheless, the temperature of 298 K was selected in further experiments because raising the temperature from 298 to 338 K would result in additional energy costs.

The concentration of H_2O_2 is also a significant factor in generating $HO^{\bullet}$ for AO7 oxidation and its effect is depicted in Figure 3c. As the concentration of H_2O_2 increased from 5.5 to 22 mM, the AO7 oxidation increased from 80 to 98% (Figure 3c). The increased degradation of AO7 results from the increased $HO^{\bullet}$ concentration. As the concentration of H_2O_2 increased further to 33 mM, the degradation of AO7 decreased to 82%. The result suggests that the excess H_2O_2 could lead to a reaction between H_2O_2 with $HO^{\bullet}$ generating hydroperoxyl radicals ($HOO^{\bullet}$).[37]

The degradation performances of AO7 at different pH experimental conditions are shown in Figure 3d. Clearly, the best degradation performances of AO7 are reached at pH = 3. When the pH value was higher than 3, the AO7 degradation decreased. This can be attributed to the decomposition of more H_2O_2 into water and oxygen without the generation of appreciable amounts of $HO^{\bullet}$. When the pH value was lower than 3, the degradation of AO7 also decreased. The results suggest that the excess H^+ lead to a scavenging effect of $HO^{\bullet}$, thus reducing the degradation reaction.

On the basis of the above results, the optimized experimental condition for AO7 degradation are [AO7] = 0.1 mM, [H_2O_2] = 22 mM, pH = 3, and T = 298 K.

Catalytic Activity of Cellulose/GO/Fe_3O_4 Hydrogels. The degradation of AO7 by H_2O_2 catalyzed with the cellulose/GO (8%)/Fe_3O_4 composite can be analytical tracked by the change in the UV−vis absorption spectrum over the course of degradation (Figure 4a). The UV−vis spectrum of the chromophore AO7 is characterized by absorptions at 430 and 484 nm, which are caused by the azo and hydrazine form, respectively. The other two peaks at 230 and 310 nm are caused by the adjacent auxochrome benzene and naphthalene rings, respectively.[38] These four characteristic peaks decreased significantly with increasing reaction time, which was attributed to the destruction of the auxochromic and chromophoric structures during the heterogeneous Fenton-like reactions.

The catalytic activity of different composites in degrading the AO7 dye is presented in Figure 4b. Insignificant degradation of the AO7 dye was observed in the presence of H_2O_2 only. The result in the blank conditions of the Fenton-like reaction could be because of the higher oxidation potential of $HO^{\bullet}$ radicals compared to H_2O_2. In the presence of cellulose/Fe_3O_4 and cellulose/GO (8%) composites, the AO7 dye was degraded by 64 and 23% after 180 min of reaction, respectively. In the presence of different cellulose/GO/Fe_3O_4 composites, the degradation degree of AO7 varied within the range of 71−98% after 180 min.

The increase in degradation rate is because of the synergistic effects between Fe_3O_4 nanoparticles and GO sheets. First, GO features aromatic ring structures that are facilitated through

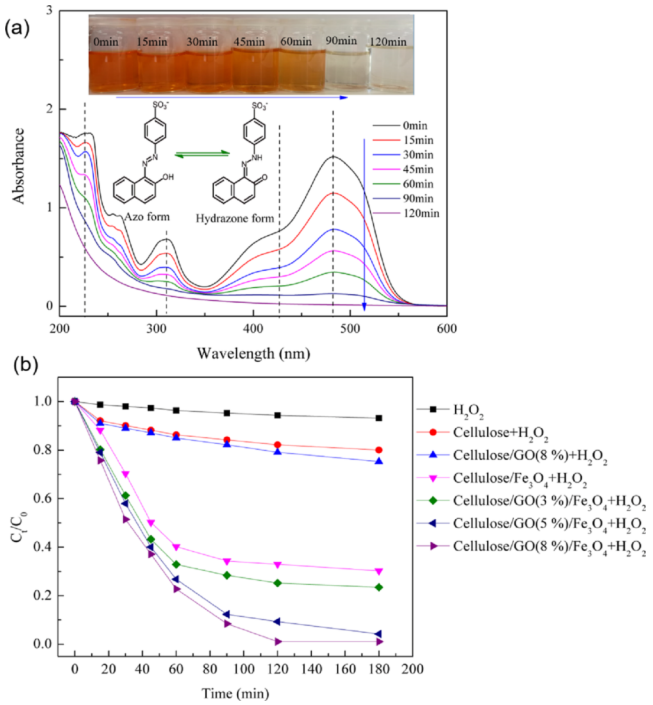

Figure 4. (a) UV−vis analysis of the degradation of AO7 by H_2O_2 catalyzed with the cellulose/GO (8%)/Fe_3O_4 composite. (b) Effect of catalysts on degradation profiles of AO7 ([AO7] = 0.1 mM, [catalyst] = 0.2 g L^{-1}, pH = 3, [H_2O_2] = 22 mM, and T = 298 K).

$\pi-\pi$ interactions and the adsorption of AO7, which contains also aromatic units (Figure 4a). This could provide an increase of AO7 concentration[39] near the active sites, and the accumulated AO7 will be oxidized faster by the $HO^{\bullet}$ generated from H_2O_2 in the direct neighborhood.[18] Second, the interactions between GO sheets and Fe_3O_4 nanoparticles could generate the electron transport between Fe_3O_4 and GO.[40] Third, the partial reduction of GO promotes the regeneration of Fe^{2+} during the degradation reaction, which enables electron transport to accelerate the redox cycle. In summary, the structural and morphological interactions of cellulose/GO/Fe_3O_4 composites determine the high catalytic activity for the degradation of AO7.

The durability of the cellulose/GO/Fe_3O_4 catalyst for the degradation of AO7 was also verified (Figure 5a). The degradation of AO7 was monitored for twenty consecutive cycles, with each cycle lasting 3 h. Before the addition of fresh AO7 solution in each cycle, cellulose/GO/Fe_3O_4 hydrogel was taken out of the solution and washed thoroughly with water. There was only very small decrease in the degradation rate during the five consecutive cycles, and even in the 20th cycle only a small decrease in degradation efficiency was detected, indicating the good stability of the prepared cellulose/GO/Fe_3O_4 catalyst.

Compared to the cellulose/Fe_3O_4 composites, as shown in Figure 5b, the cellulose/GO (8%)/Fe_3O_4 composites exhibited excellent catalytic stability over five cycles, with unobvious AO7 degradation efficiency lost. Conversely, the degradation activity of cellulose/Fe_3O_4 composites declines quickly. While in the first cycle, 64% of AO7 were decomposed, the efficiency of cellulose/Fe_3O_4 composites decreased to only 14% AO7 degradation in the fifth cycle. The catalytic stability of cellulose/GO/Fe_3O_4 composites over several cycles (even twenty cycles) resulted from the co-effect between Fe_3O_4 and

DOI: 10.1021/acsomega.9b00170
ACS Omega 2019, 4, 5117−5125

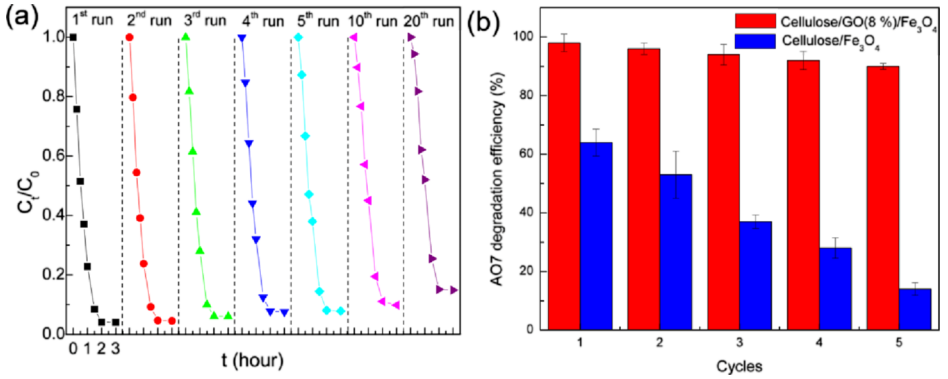

Figure 5. (a) Cycling runs in the AO7 degradation using cellulose/GO (8%)/Fe_3O_4 composites. (b) Comparison of the long-term stability of the catalytic activity of the cellulose/GO/Fe_3O_4 and cellulose/Fe_3O_4 composites tested by repeated use for AO7 degradation.

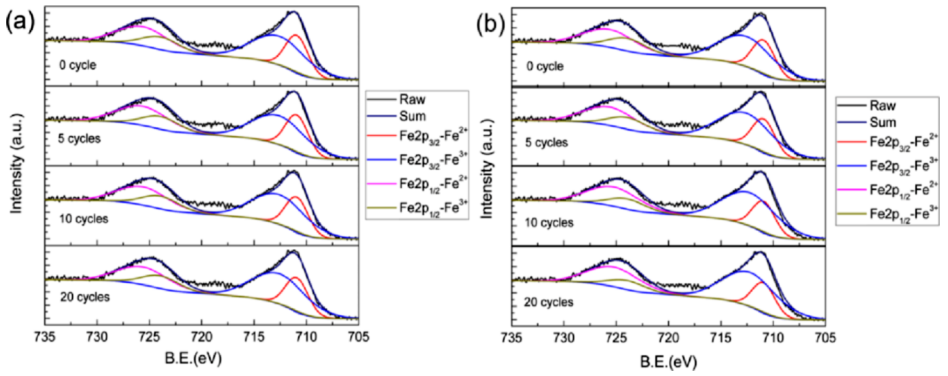

Figure 6. XPS spectra of (a) cellulose/GO (8%)/Fe_3O_4 composites and (b) cellulose/Fe_3O_4 composites during 20 cycles.

Table 1. Fe^{3+}/Fe^{2+} Ratio of Cellulose/GO (8%)/Fe_3O_4 and Cellulose/Fe_3O_4 Composites during 20 Cycles

		Fe $2p_{1/2}$		Fe $2p_{3/2}$		
samples	cycles	Fe^{3+} (%)	Fe^{2+} (%)	Fe^{3+} (%)	Fe^{2+} (%)	Fe^{3+}/Fe^{2+} ratio
cellulose/GO/Fe_3O_4	0	22.14	8.14	44.75	24.97	2.02
	1	21.42	7.36	45.47	25.75	2.02
	3	22.56	8.01	44.22	25.21	2.01
	5	22.43	7.95	44.23	25.38	2.00
	10	22.44	7.75	44.45	25.36	2.02
	20	22.98	8.10	43.41	25.51	2.05
cellulose/Fe_3O_4	0	22.01	7.77	44.77	25.45	2.02
	1	21.95	8.45	48.11	21.49	2.34
	3	22.43	8.35	49.48	19.74	2.56
	5	21.87	6.14	53.98	18.01	3.14
	10	24.19	3.60	55.36	16.85	3.89
	20	24.90	3.62	57.12	14.36	4.56

GO. The counter-intuitive result was due to the loss of surface passivation of cellulose/GO/Fe_3O_4 hydrogels. In the system, the surface passivation of cellulose/GO/Fe_3O_4 hydrogel might be prevented by the effective formation of $HO^{\bullet}$.[41,42] In cellulose/Fe_3O_4 hydrogels, the ineffective regeneration of Fe^{2+} during the degradation reaction could bring about the generation of passivated Fe_3O_4,[18,43] resulting in a loss of catalytic activity.

XPS analysis was carried out to clarify the possible regeneration of Fe^{2+} of cellulose/GO/Fe_3O_4 and cellulose/Fe_3O_4 composites. The Fe 2p spectra of cellulose/GO (8%)/Fe_3O_4 composites and cellulose/Fe_3O_4 composites (see Figure 6) showed the spin−orbit doublets of Fe $2p_{1/2}$ at 724.6 eV and Fe $2p_{3/2}$ at 711.1 eV. The deconvolution of Fe^{2+} and Fe^{3+} confirms the regeneration of Fe^{2+} by quantifying the changes in the Fe^{3+}/Fe^{2+} ratio. Table 1 summarized the details of Fe^{2+} and Fe^{3+} peaks in regard to their ratio. An apparent increase in the Fe^{3+}/Fe^{2+} ratio after twenty catalysis cycles was only found in the cellulose/Fe_3O_4 composites rather than the cellulose/GO/Fe_3O_4 composites. The increase in the Fe^{3+}/Fe^{2+} ratio from 2.02 to 4.56 in cellulose/Fe_3O_4 is due to a proportion of the Fe^{2+} being oxidized into Fe^{3+} on the surface of Fe_3O_4 nanoparticles throughout the catalysis. On the contrary, no increase in the ratio of Fe^{3+}/Fe^{2+} was observed for the cellulose/GO/Fe_3O_4 composites. These results plausibly confirmed the ineffective regeneration of Fe^{2+} in cellulose/Fe_3O_4 composites during degradation reaction of AO7 and the good regeneration of Fe^{2+} of cellulose/GO/Fe_3O_4 composites,

DOI: 10.1021/acsomega.9b00170
ACS Omega 2019, 4, 5117−5125

which was associated with the presence of synergistic interactions between Fe_3O_4 nanoparticles and GO during the heterogeneous Fenton-like reaction. In fact, these results are also related to the high performance of cellulose/GO/Fe_3O_4 composites in removal of AO7 during the long-term stability test (Figure 5).

As mentioned above, the cellulose/GO/Fe_3O_4 composites as the catalyst exhibit outstanding durability and recyclability. To explain this phenomenon, Figure 7 presents the proposed mechanism of synergy of Fe_3O_4 and GO in delivering the excellent and durability performance. First, the degradation of AO7 mainly takes place at the solid−liquid interface, where the generation of $HO^{\bullet}$ radicals is caused by the decomposition of the adsorbed H_2O_2 by the actives sites of the Fe_3O_4 nanoparticles coated on the surface of GO (eq 1 and 2). Second, in addition to the active sites (Fe^{2+}/Fe^{3+}) of Fe_3O_4 nanoparticles, H_2O_2 could also be decomposed on the surface of GO to generate $HO^{\bullet}$ radicals,[44] which result from the donor−acceptor properties of GO sheets[45−48] based on an electron-transfer mechanism (eq 3 and 4). Third, π electrons on the surface of GO in turn can generate the electron transfer between Fe_3O_4 and GO,[40] which result from the existence of many semiconducting π-conjugated sp^2 carbon domains.[49] The feasibility of the electron transfer can be ascribed to the standard reduction potential of GO (−0.19 V),[50] which is lower than that of Fe^{3+}/Fe^{2+} (+0.771 V).[21,45] Therefore, the spontaneous reduction from Fe^{3+} to Fe^{2+} could be available because the electron donation from the GO sheets to the oxidized active sites. Because the regeneration of Fe^{2+} by H_2O_2 (eq 2) was quite slow, this synergistic effect between Fe_3O_4 nanoparticles and GO is beneficial in speeding up the redox cycles (eq 5).[29] The fast regeneration of Fe^{2+} is greatly promoting the decomposition of H_2O_2. Finally, the hydrogel structure of cellulose/GO/Fe_3O_4, which consists of multiple hydrogen bonds, ensures the stability of every component after many catalysis cycles. Overall, the electron transfer in the cellulose/GO/Fe_3O_4 hydrogel plays the major role in the redox reaction of Fe_3O_4 nanoparticles, which can achieve the good and long-lasting degradation performance of AO7.

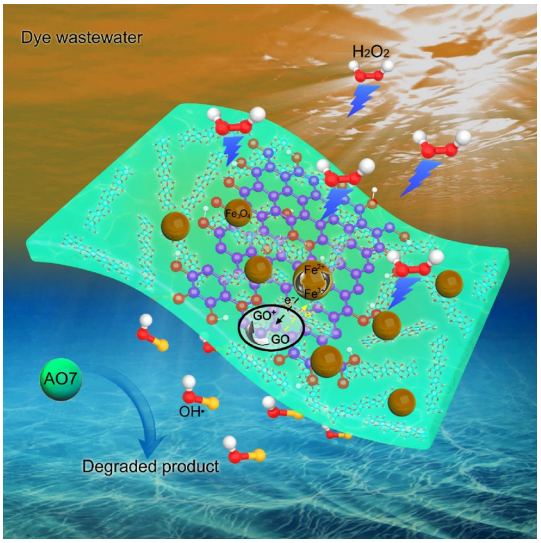

Figure 7. Proposed mechanism of the cellulose/GO/Fe_3O_4 hydrogel as the catalyst to degrade AO7.

$$Fe^{2+} + H_2O_2 \rightarrow Fe^{3+} + HO^{\bullet} + OH^{-} \quad (1)$$

$$Fe^{3+} + H_2O_2 \rightarrow Fe^{2+} + HOO^{\bullet} + H^{+} \quad (2)$$

$$GO_{C=C\ sp^2} + H_2O_2 \rightarrow GO_{C-C\ sp^3} + HO^{\bullet} + OH^{-} \quad (3)$$

$$GO_{C-C\ sp^3} + H_2O_2 \rightarrow GO_{C=C\ sp^2} + HOO^{\bullet} + H^{+} \quad (4)$$

$$GO_{C=C\ sp^2} + Fe^{3+} \rightarrow GO_{C-C\ sp^3} + Fe^{2+} \quad (5)$$

In order to have a rough estimation of the efficiency of cellulose/GO/Fe_3O_4 hydrogels as the catalyst to degrade AO7, the degradation performance and stability were compared with those reported in the literature. Table 2 contains different catalysts able to degrade AO7 dye at similar operational conditions. Under this condition, most of the recent reports have lower removal percentage of AO7 than the ones reported here. Compared to them, the cellulose/GO/Fe_3O_4 hydrogel exhibited good degradation performance and excellent recyclability. Only the system described in ref 53 shows similar behavior compared to our cellulose-based system. Moreover, another advantage of the hydrogel as the catalyst is that the cellulose matrix contains GO and Fe_3O_4 nanoparticles and maintains the hydrogel structure during the catalyst reaction, which will not result in secondary pollution. The "dip-catalyst" can be easily removed from the polluted water

Table 2. Degradation Performance and Stability of Different Systems

dyes	catalyst	percentage of removal	stability	conditions	refs
AO7	GO/Fe_3O_4	80.0% in 20 min		pH 3; 0.1 mM dye; 22 mM H_2O_2; 298 K	30
		98.0% in 180 min			
AO7	BiOI/$ZnFe_2O_4$	90.5% in 180 min		pH 5; 20 mg L^{-1} dye; 298 K	51
AO7	pillared saponite clay impregnated with Fe(II)acetylacetonate	91.8% in 180 min		pH 5; 0.1 mM dye; 20 mM H_2O_2; 303 K	52
AO7	BiOI−BiOCl/C_3N_4	96.6% in 140 min	87.4% in 140 min after the 4th run	pH 6; 0.1 mM dye; 20 mM H_2O_2; 303 K	53
AO7	CdO−ZnO	69% in 140 min		pH 7; 20 mg L^{-1} dye; 298 K	54
AO7	Cd−TiO_2	95% in 120 min		pH 2; 20 mg L^{-1} dye; 298 K	55
AO7	Ag−ZnO/CNT	98% in 120 min	95% in 120 min after the 4th run	pH 5; 20 mg L^{-1} dye; 298 K	56
AO7	cellulose/GO (8%)/Fe_3O_4 hydrogel	97% in 120 min	90% in 180 min after the 20th run	pH 3; 0.1 mM dye; 22 mM H_2O_2; 298 K	this work
		98% in 180 min			

DOI: 10.1021/acsomega.9b00170
ACS Omega 2019, 4, 5117−5125

after the degradation reaction. In other words, it is easy to start and stop the degradation reaction by taking in and out the whole hydrogel. It is obvious that the cellulose/GO/Fe_3O_4 hydrogel, with its sustainable feature, convenient fabrication, great catalytic efficiency, good recyclability, and easy removability, is expected to be very useful in AO7 dye removal.

CONCLUSIONS

In conclusion, we have successfully grown Fe_3O_4 nanoparticles on cellulose/GO hydrogels by a simple, scalable, and facile method. This method produced cellulose/GO/Fe_3O_4 composites, in which Fe_3O_4 nanoparticles were uniformly and densely coated on the surface of GO and cellulose chains. The resulting composites show superior and durable catalytic activity in oxidation of AO7 dye compared to cellulose/Fe_3O_4 composites, which results from the synergistic effect of Fe_3O_4 and GO. We expect that the composite hydrogels can be also useful for the purification of other dye-contaminated wastewaters. Our method could be further extended to grow other functional materials on cellulose or cellulose/GO composites for advanced applications.

EXPERIMENTAL SECTION

Materials. The cellulose samples are cotton linters, DP 500, supplied by Hubei Chemical Fiber Group Ltd. (Xiangfan, China). AO7 (orange II; 85%), GO dispersion (4 mg/mL), $FeCl_2{\cdot}4H_2O$ (99%), and $FeCl_3{\cdot}6H_2O$ (97%) were purchased from Sigma-Aldrich and used as received.

Preparation of Cellulose/GO Composite Hydrogels. A solution of NaOH/urea/H_2O (7:12:81 by weight) was prepared as solvent. The designated amounts of NaOH and urea were added into distilled water and then the solvent was precooled to −12 °C. The designated amount of cellulose was added and dissolved into the solvent under vigorous stirring for 5 min. Then, a calculated amount of GO dispersion (4 mg/mL, Sigma-Aldrich) was added into the cellulose solution under vigorous stirring for 5 min. After degasification, the mixture was cast on a glass plate to give a 400 μm thick gel sheet, which was then immersed into a coagulation bath with 5 wt % H_2SO_4 for 5 min at room temperature to coagulate and regenerate. It was then immersed in distilled water to remove urea and NaOH.

By adjustment of the amount of the GO aqueous dispersion, cellulose/GO composite hydrogels consisting of 100 g water, 4 g cellulose, and different GO contents of 3, 5, and 8 wt %, related to the cellulose amount were obtained.

Preparation of Cellulose/GO/Fe_3O_4 and Cellulose/Fe_3O_4 Composite Hydrogels. The cellulose/GO hydrogel was immersed into an aqueous solution (200 mL) consisting of 8 mmol $FeCl_3{\cdot}6H_2O$ and 4 mmol $FeCl_2{\cdot}4H_2O$ for 2 h at room temperature. Subsequently, the cellulose/GO hydrogel was added into the NaOH (1 M) solution for another 5 min. The resultant hydrogels were washed with running water and deionized water.

Characterization of Morphology and Microstructure of Composite Films. For the characterization of the composites, the hydrogels were fixed on glass plates using Scotch tape and dried at ambient temperature to obtain films with a thickness of ca 40 μm. Transmission electron microscopy (TEM) was performed using a LIBRA 200 MC (Carl Zeiss SMT, Oberkochen, Germany) at an accelerating voltage of 200 kV. The films were embedded in epoxy resin, and ultrathin sections with a thickness of about 90 nm were cut with an ultrasonic diamond knife (DIATOME, Switzerland) by using ultramicrotome EM UC/FC 6 of the company Leica (Austria) at room temperature. XRD was performed using a D/MAX-1200 (Rigaku Co., Japan) with a wavelength of 0.154 nm and a Lynx Eye detector at a scanning rate of 2θ = 1° min^{-1}. X-ray photoelectron spectroscopy (XPS) was performed using a Kratos Axis ULTRA X-ray photoelectron spectrometer with monochromatic Al Kα ($h\nu$ = 1486.6 eV). All XPS spectra were corrected using the C 1s line at 284.6 eV. FTIR spectroscopy in the range of 4000−500 cm^{-1} was performed on a Spectrum 400 FT-IR/ATR Spectrometer (PerkinElmer, USA). Thermogravimetric analysis (TGA) was done using a TGA Q5000 (TA Instruments, USA) from 30 to 800 °C with an increment of 10 K min^{-1}.

Testing of Catalytic Activity. First, the cellulose/GO (8%)/Fe_3O_4 hydrogel was chosen to study in detail the effect of the parameters initial AO7 dye concentration, temperature, pH, and the initial concentration of H_2O_2 on the catalytic performance. Hydrogel (5 g) in the shape of a thick film of about 120 × 80 × 0.5 mm^3 were dipped into 250 mL solution of AO7 and the AO7 degradation was followed with time. The experimental design was chosen by changing one factor and keeping the others constant. The variation of parameters was chosen as follows: AO7 concentration = 0.1, 0.2, 0.3, and 0.4 mM; H_2O_2 concentration = 5.5, 11, 22, and 33 mM; pH = 2, 2.5, 3, 3.5, and 4; temperature = 298, 318, and 338 K.

Then, so as to compare the degradation performance of different cellulose/GO/Fe_3O_4, cellulose/GO, and cellulose/Fe_3O_4 hydrogels, the catalytic activity of AO7 was studied using the different hydrogels at constant conditions with AO7 aqueous solutions of 250 mL (experimental conditions: [AO7] = 0.1 mM, [catalyst] = 0.2 g L^{-1}, pH = 3, [H_2O_2] = 22 mM, and T = 298 K). The initial pH of the AO7 solution was adjusted to 3. The reactions were initiated by adding H_2O_2 (22 mM) into the suspension. It should be noted that, before the reaction, the solution was stirred in the dark for 30 min to achieve the adsorption equilibrium. The concentration of AO7 was analyzed by spectrophotometer at a wavelength of 484 nm. The UV−vis spectra of the samples were recorded in air atmosphere at room temperature from 200 to 600 nm using a UV−vis spectrophotometer (SPECORD 201 PLUS, Analytik Jena, Germany).

ASSOCIATED CONTENT

Supporting Information

The Supporting Information is available free of charge on the ACS Publications website at DOI: 10.1021/acsomega.9b00170.

Wide-scan XPS spectra and high-resolution Fe 2p spectra of different nanocomposites and Fe_3O_4 nanoparticles and TGA curves of different composites and cellulose and residues of cellulose/GO and cellulose/GO/Fe_3O_4 composites (PDF)

AUTHOR INFORMATION

Corresponding Authors

*E-mail: poe@ipfdd.de (P.P.).
*E-mail: qihs@scut.edu.cn (H.Q.).

ORCID

Petra Pötschke: 0000-0001-6392-7880
Jürgen Pionteck: 0000-0003-2310-1106

DOI: 10.1021/acsomega.9b00170
ACS Omega 2019, 4, 5117−5125

Brigitte Voit: 0000-0002-4531-691X
Haisong Qi: 0000-0001-7493-3573

Author Contributions

The manuscript was written through contributions of all authors. All authors have given approval to the final version of the manuscript.

Notes

The authors declare no competing financial interest.

■ ACKNOWLEDGMENTS

We would like to thank Mrs. Reuter for TEM observation, Mrs. Pilch for UV−vis spectrophotometer testing as well as Dr. Simon for XPS characterization (all from IPF). Y.C. appreciates the funding from China Scholarship Council (grant 201606240112) for the PhD study at Leibniz-Institut für Polymerforschung Dresden e.V. H.Q. thanks the National Natural Science Foundation of China (grant 21774036) for the financial support of this work.

■ REFERENCES

(1) Chan, S. H. S.; Wu, T. Y.; Juan, J. C.; Teh, C. Y. Recent developments of metal oxide semiconductors as photocatalysts in advanced oxidation processes (AOPs) for treatment of dye waste-water. *J. Chem. Technol. Biotechnol.* **2011**, *86*, 1130−1158.

(2) Devi, L. G.; Kumar, S. G.; Reddy, K. M.; Munikrishnappa, C. Photo degradation of Methyl Orange an azo dye by Advanced Fenton Process using zero valent metallic iron: Influence of various reaction parameters and its degradation mechanism. *J. Hazard. Mater.* **2009**, *164*, 459−467.

(3) Sun, S.-P.; Li, C.-J.; Sun, J.-H.; Shi, S.-H.; Fan, M.-H.; Zhou, Q. Decolorization of an azo dye Orange G in aqueous solution by Fenton oxidation process: effect of system parameters and kinetic study. *J. Hazard. Mater.* **2009**, *161*, 1052−1057.

(4) Ramirez, J. H.; Duarte, F. M.; Martins, F. G.; Costa, C. A.; Madeira, L. M. Modelling of the synthetic dye Orange II degradation using Fenton's reagent: From batch to continuous reactor operation. *Chem. Eng. J.* **2009**, *148*, 394−404.

(5) Riaz, N.; Chong, F. K.; Dutta, B. K.; Man, Z. B.; Khan, M. S.; Nurlaela, E. Photodegradation of Orange II under visible light using Cu-Ni/TiO2: Effect of calcination temperature. *Chem. Eng. J.* **2012**, *185-186*, 108−119.

(6) Ember, E.; Rothbart, S.; Puchta, R.; van Eldik, R. Metal ion-catalyzed oxidative degradation of Orange II by H_2O_2. High catalytic activity of simple manganese salts. *New J. Chem.* **2009**, *33*, 34−49.

(7) Li, G.; Qu, J.; Zhang, X.; Liu, H.; Liu, H. Electrochemically assisted photocatalytic degradation of Orange II: influence of initial pH values. *J. Mol. Catal. A: Chem.* **2006**, *259*, 238−244.

(8) Herney-Ramirez, J.; Lampinen, M.; Vicente, M. A.; Costa, C. A.; Madeira, L. M. Experimental design to optimize the oxidation of Orange II dye solution using a clay-based Fenton-like catalyst. *Ind. Eng. Chem. Res.* **2008**, *47*, 284−294.

(9) Ramirez, J. H.; Costa, C. A.; Madeira, L. M.; Mata, G.; Vicente, M. A.; Rojas-Cervantes, M. L.; López-Peinado, A. J.; Martín-Aranda, R. M. Fenton-like oxidation of Orange II solutions using heterogeneous catalysts based on saponite clay. *Appl. Catal., B* **2007**, *71*, 44−56.

(10) Herney-Ramirez, J.; Silva, A. M. T.; Vicente, M. A.; Costa, C. A.; Madeira, L. M. Degradation of Acid Orange 7 using a saponite-based catalyst in wet hydrogen peroxide oxidation: Kinetic study with the Fermi's equation. *Appl. Catal., B* **2011**, *101*, 197−205.

(11) Hassan, H.; Hameed, B. H. Fe-clay as effective heterogeneous Fenton catalyst for the decolorization of Reactive Blue 4. *Chem. Eng. J.* **2011**, *171*, 912−918.

(12) Garrido-Ramírez, E. G.; Theng, B. K. G.; Mora, M. L. Clays and oxide minerals as catalysts and nanocatalysts in Fenton-like reactions - A review. *Appl. Clay Sci.* **2010**, *47*, 182−192.

(13) Hsueh, C.; Huang, Y.; Chen, C. Novel activated alumina-supported iron oxide-composite as a heterogeneous catalyst for photooxidative degradation of reactive black 5. *J. Hazard. Mater.* **2006**, *129*, 228−233.

(14) Lim, H.; Lee, J.; Jin, S.; Kim, J.; Yoon, J.; Hyeon, T. Highly active heterogeneous Fenton catalyst using iron oxide nanoparticles immobilized in alumina coated mesoporous silica. *Chem. Commun.* **2006**, 463−465.

(15) Rache, M. L.; García, A. R.; Zea, H. R.; Silva, A. M. T.; Madeira, L. M.; Ramírez, J. H. Azo-dye orange II degradation by the heterogeneous Fenton-like process using a zeolite Y-Fe catalyst-Kinetics with a model based on the Fermi's equation. *Appl. Catal., B* **2014**, *146*, 192−200.

(16) Aleksić, M.; Kušić, H.; Koprivanac, N.; Leszczynska, D.; Božić, A. L. Heterogeneous Fenton type processes for the degradation of organic dye pollutant in water—The application of zeolite assisted AOPs. *Desalination* **2010**, *257*, 22−29.

(17) Gan, P. P.; Li, S. F. Y. Efficient removal of Rhodamine B using a rice hull-based silica supported iron catalyst by Fenton-like process. *Chem. Eng. J.* **2013**, *229*, 351−363.

(18) Hu, X.; Liu, B.; Deng, Y.; Chen, H.; Luo, S.; Sun, C.; Yang, P.; Yang, S. Adsorption and heterogeneous Fenton degradation of 17α-methyltestosterone on nano Fe3O4/MWCNTs in aqueous solution. *Appl. Catal., B* **2011**, *107*, 274−283.

(19) Zhou, L.; Zhang, H.; Ji, L.; Shao, Y.; Li, Y. Fe3O4/MWCNT as a heterogeneous Fenton catalyst: degradation pathways of tetrabromobisphenol A. *RSC Adv.* **2014**, *4*, 24900−24908.

(20) Ramirez, J. H.; Maldonado-Hódar, F. J.; Pérez-Cadenas, A. F.; Moreno-Castilla, C.; Costa, C. A.; Madeira, L. M. Azo-dye Orange II degradation by heterogeneous Fenton-like reaction using carbon-Fe catalysts. *Appl. Catal., B* **2007**, *75*, 312−323.

(21) Song, S.; Rao, R.; Yang, H.; Liu, H.; Zhang, A. Facile synthesis of Fe_3O_4/MWCNTs by spontaneous redox and their catalytic performance. *Nanotechnology* **2010**, *21*, 185602.

(22) Wang, Z.; Ai, L.; Huang, Y.; Zhang, J.; Li, S.; Chen, J.; Yang, F. Degradation of azo dye with activated peroxygens: when zero-valent iron meets chloride. *RSC Adv.* **2017**, *7*, 30941−30948.

(23) Nguyen, T. D.; Phan, N. H.; Do, M. H.; Ngo, K. T. Magnetic Fe_2MO_4 (M: Fe, Mn) activated carbons: fabrication, characterization and heterogeneous Fenton oxidation of methyl orange. *J. Hazard. Mater.* **2011**, *185*, 653−661.

(24) Rodríguez, A.; Ovejero, G.; Sotelo, J.; Mestanza, M.; García, J. Heterogeneous Fenton catalyst supports screening for mono azo dye degradation in contaminated wastewaters. *Ind. Eng. Chem. Res.* **2010**, *49*, 498−505.

(25) Deng, J.; Wen, X.; Wang, Q. Solvothermal in situ synthesis of Fe_3O_4-multi-walled carbon nanotubes with enhanced heterogeneous Fenton-like activity. *Mater. Res. Bull.* **2012**, *47*, 3369−3376.

(26) Duan, F.; Yang, Y.; Li, Y.; Cao, H.; Wang, Y.; Zhang, Y. Heterogeneous Fenton-like degradation of 4-chlorophenol using iron/ordered mesoporous carbon catalyst. *J. Environ. Sci.* **2014**, *26*, 1171−1179.

(27) Duarte, F.; Maldonado-Hódar, F. J.; Pérez-Cadenas, A. F.; Madeira, L. M. Fenton-like degradation of azo-dye Orange II catalyzed by transition metals on carbon aerogels. *Appl. Catal., B* **2009**, *85*, 139−147.

(28) Voitko, K. V.; Whitby, R. L. D.; Gun'ko, V. M.; Bakalinska, O. M.; Kartel, M. T.; Laszlo, K.; Cundy, A. B.; Mikhalovsky, S. V. Morphological and chemical features of nano and macroscale carbons affecting hydrogen peroxide decomposition in aqueous media. *J. Colloid Interface Sci.* **2011**, *361*, 129−136.

(29) Zubir, N. A.; Yacou, C.; Motuzas, J.; Zhang, X.; Da Costa, J. D. Structural and functional investigation of graphene oxide-Fe_3O_4 nanocomposites for the heterogeneous Fenton-like reaction. *Sci. Rep.* **2014**, *4*, 4594.

(30) Zubir, N. A.; Yacou, C.; Zhang, X.; Diniz da Costa, J. C.; Da Costa, J. D. Optimisation of graphene oxide-iron oxide nano-composite in heterogeneous Fenton-like oxidation of Acid Orange 7. *J. Environ. Chem. Eng.* **2014**, *2*, 1881−1888.

DOI: 10.1021/acsomega.9b00170
ACS Omega 2019, 4, 5117−5125

(31) Zubir, N. A.; Zhang, X.; Yacou, C.; Diniz da Costa, J. C. Fenton-Like degradation of acid orange 7 using graphene oxide-iron oxide nanocomposite. *Sci. Adv. Mater.* **2014**, *6*, 1382−1388.
(32) Yang, X.; Zhang, X.; Ma, Y.; Huang, Y.; Wang, Y.; Chen, Y. Superparamagnetic graphene oxide−Fe_3O_4 nanoparticles hybrid for controlled targeted drug carriers. *J. Mater. Chem.* **2009**, *19*, 2710−2714.
(33) He, H.; Gao, C. Supraparamagnetic, conductive, and processable multifunctional graphene nanosheets coated with high-density Fe_3O_4 nanoparticles. *ACS Appl. Mater. Interfaces* **2010**, *2*, 3201−3210.
(34) Chandra, V.; Park, J.; Chun, Y.; Lee, J. W.; Hwang, I.-C.; Kim, K. S. Water-dispersible magnetite-reduced graphene oxide composites for arsenic removal. *ACS Nano* **2010**, *4*, 3979−3986.
(35) Liu, M.; Chen, C.; Hu, J.; Wu, X.; Wang, X. Synthesis of Magnetite/Graphene Oxide Composite and Application for Cobalt-(II) Removal. *J. Phys. Chem. C* **2011**, *115*, 25234−25240.
(36) Wu, H.; Gao, G.; Zhou, X.; Zhang, Y.; Guo, S. Control on the formation of Fe_3O_4 nanoparticles on chemically reduced graphene oxide surfaces. *CrystEngComm* **2012**, *14*, 499−504.
(37) Ramirez, J. H.; Costa, C. A.; Madeira, L. M. Experimental design to optimize the degradation of the synthetic dye Orange II using Fenton's reagent. *Catal. Today* **2005**, *107-108*, 68−76.
(38) Stankovich, S.; Dikin, D. A.; Dommett, G. H. B.; Kohlhaas, K. M.; Zimney, E. J.; Stach, E. A.; Piner, R. D.; Nguyen, S. T.; Ruoff, R. S. Graphene-based composite materials. *Nature* **2006**, *442*, 282−286.
(39) Qu, J.-c.; Ren, C.-l.; Dong, Y.-l.; Chang, Y.-p.; Zhou, M.; Chen, X.-g. Facile synthesis of multifunctional graphene oxide/AgNPs-Fe_3O_4 nanocomposite: a highly integrated catalysts. *Chem. Eng. J.* **2012**, *211-212*, 412−420.
(40) Jasuja, K.; Linn, J.; Melton, S.; Berry, V. Microwave-reduced uncapped metal nanoparticles on graphene: tuning catalytic, electrical, and Raman properties. *J. Phys. Chem. Lett.* **2010**, *1*, 1853−1860.
(41) Xue, X.; Hanna, K.; Abdelmoula, M.; Deng, N. Adsorption and oxidation of PCP on the surface of magnetite: kinetic experiments and spectroscopic investigations. *Appl. Catal., B* **2009**, *89*, 432−440.
(42) Rusevova, K.; Kopinke, F.-D.; Georgi, A. Nano-sized magnetic iron oxides as catalysts for heterogeneous Fenton-like reactions-Influence of Fe(II)/Fe(III) ratio on catalytic performance. *J. Hazard. Mater.* **2012**, *241-242*, 433−440.
(43) Bokare, A. D.; Chikate, R. C.; Rode, C. V.; Paknikar, K. M. Iron-nickel bimetallic nanoparticles for reductive degradation of azo dye Orange G in aqueous solution. *Appl. Catal., B* **2008**, *79*, 270−278.
(44) Zhang, W.; Wang, C.; Li, Z.; Lu, Z.; Li, Y.; Yin, J.-J.; Zhou, Y.-T.; Gao, X.; Fang, Y.; Nie, G. Unraveling Stress-Induced Toxicity Properties of Graphene Oxide and the Underlying Mechanism. *Adv. Mater.* **2012**, *24*, 5391−5397.
(45) Song, S.; Yang, H.; Rao, R.; Liu, H.; Zhang, A. High catalytic activity and selectivity for hydroxylation of benzene to phenol over multi-walled carbon nanotubes supported Fe_3O_4 catalyst. *Appl. Catal., A* **2010**, *375*, 265−271.
(46) Domínguez, C. M.; Ocón, P.; Quintanilla, A.; Casas, J. A.; Rodriguez, J. J. Highly efficient application of activated carbon as catalyst for wet peroxide oxidation. *Appl. Catal., B* **2013**, *140-141*, 663−670.
(47) Domínguez, C. M.; Quintanilla, A.; Ocón, P.; Casas, J. A.; Rodriguez, J. J. The use of cyclic voltammetry to assess the activity of carbon materials for hydrogen peroxide decomposition. *Carbon* **2013**, *60*, 76−83.
(48) Lücking, F.; Köser, H.; Jank, M.; Ritter, A. Iron powder, graphite and activated carbon as catalysts for the oxidation of 4-chlorophenol with hydrogen peroxide in aqueous solution. *Water Res.* **1998**, *32*, 2607−2614.
(49) Matsumoto, Y.; Koinuma, M.; Ida, S.; Hayami, S.; Taniguchi, T.; Hatakeyama, K.; Tateishi, H.; Watanabe, Y.; Amano, S. Photoreaction of graphene oxide nanosheets in water. *J. Phys. Chem. C* **2011**, *115*, 19280−19286.
(50) Karousis, N.; Sandanayaka, A. S. D.; Hasobe, T.; Economopoulos, S. P.; Sarantopoulou, E.; Tagmatarchis, N. Graphene oxide with covalently linked porphyrin antennae: Synthesis, characterization and photophysical properties. *J. Mater. Chem.* **2011**, *21*, 109−117.
(51) Yosefi, L.; Haghighi, M.; Allahyari, S. Solvothermal synthesis of flowerlike p-BiOI/n-$ZnFe_2O_4$ with enhanced visible light driven nanophotocatalyst used in removal of acid orange 7 from wastewater. *Sep. Purif. Technol.* **2017**, *178*, 18−28.
(52) Herney-Ramirez, J.; Silva, A. M. T.; Vicente, M. A.; Costa, C. A.; Madeira, L. M. Degradation of Acid Orange 7 using a saponite-based catalyst in wet hydrogen peroxide oxidation: Kinetic study with the Fermi's equation. *Appl. Catal., B* **2011**, *101*, 197−205.
(53) Aghdam, S. M.; Haghighi, M.; Allahyari, S.; Yosefi, L. Precipitation dispersion of various ratios of BiOI/BiOCl nano-composite over g-C_3N_4 for promoted visible light nanophotocatalyst used in removal of acid orange 7 from water. *J. Photochem. Photobiol., A* **2017**, *338*, 201−212.
(54) Margan, P.; Haghighi, M. Sono-coprecipitation synthesis and physicochemical characterization of CdO-ZnO nanophotocatalyst for removal of acid orange 7 from wastewater. *Ultrason. Sonochem.* **2018**, *40*, 323−332.
(55) Margan, P.; Haghighi, M. Hydrothermal-assisted sol−gel synthesis of Cd-doped TiO_2 nanophotocatalyst for removal of acid orange from wastewater. *J. Sol-Gel Sci. Technol.* **2017**, *81*, 556−569.
(56) Moradi, M.; Haghighi, M.; Allahyari, S. Precipitation dispersion of Ag-ZnO nanocatalyst over functionalized multiwall carbon nanotube used in degradation of Acid Orange from wastewater. *Process Saf. Environ. Prot.* **2017**, *107*, 414−427.

DOI: 10.1021/acsomega.9b00170
ACS Omega 2019, 4, 5117−5125